Journal of Alloys and Compounds 831 (2020) 154869

Contents lists available at ScienceDirect

Journal of Alloys and Compounds

journal homepage: http://www.elsevier.com/locate/jalcom

Research on Cs/O activation process of near-infrared $In_{0.53}Ga_{0.47}As$ photocathodes

Liang Chen [a], Yang Shen [a, *], Xiaodong Yang [b], Muchun Jin [c], Songmin Liu [d], Lingze Duan [e], Shiqing Xu [a]

[a] Institute of Optoelectronics Technology, China Jiliang University, Hangzhou, 310018, China
[b] School of Physics, Nanjing University, Nanjing, 210093, China
[c] North Night Vision Technology Co. LTD., Nanjing, 211106, China
[d] School of Electronic Science and Engineering, Nanjing University, Nanjing, 210093, China
[e] Department of Physics, The University of Alabama in Huntsville, Huntsville, AL, 35899, USA

ARTICLE INFO

Article history:
Received 11 December 2019
Received in revised form
18 March 2020
Accepted 19 March 2020
Available online 23 March 2020

Keywords:
NEA
$In_xGa_{1-x}As$ photocathodes
Photoemission
Work function
Cs/O activation

ABSTRACT

We report a systematic theoretical investigation on the activation mechanism of near-infrared $In_{0.53}Ga_{0.47}As$ photocathodes. Adsorption energies, dipole moments, work functions, density of states, band structures and electron affinity of Cs/O co-adsorption on (001) surface of $In_{0.53}Ga_{0.47}As$ photocathodes are investigated. First-principles calculation results indicate that the structural stability is greatly enhanced when oxygen atoms adsorb on the Cs-covered surface. The incorporation of oxygen atom helps lower the work function further to achieve the true NEA state. Moreover, two adatom-induced surface dipoles, namely [Cs^{n+}-$In_{0.53}Ga_{0.47}As^{n-}$] and [$Cs^{+}$-$O^{2-}$-$Cs^{+}$], are also adopted to explain the relationship between the adatoms and the substrate. The HOMO and LUMO levels can further move downward and the band bending region is enlarged after Cs/O co-activation. Meanwhile, new energy bands appear in the deep valence band due to the joint effect of Cs 5s, Cs 5p, O 2s and O 2p state electrons. Finally, Cs/O activation experiments are carried out and the photocurrent curves during activation procedure are recorded. The change of photocurrent is closely related to the work function variation, which affects the photoemission of the photocathodes. In order to clearly show the electron affinity, the variation of surface barrier height of InGaAs photocathodes with Cs/O adlayer is also given.

1. Introduction

As known, the spectral threshold and magnitude of photoemission are determined by the potential barrier on the surface and by the probability of electron escape to vacuum. The adsorption of Cs and O or NF_3 on the III-V photocathode surface reduces the surface barrier to a state of negative electron affinity (NEA) [1–6]. Owing to the role of NEA, GaAs photocathodes, with higher quantum yield values (up to ~50%) and higher spin polarization, become an appropriate candidate for the fabrication of photomultiplier tubes (PMT), spin-polarized electron sources and low-level night vision over the last half century [7–10]. Due to their adjustable ranges of spectral response, NEA AlGaAs photocathodes could also be applied to the electron accelerators due to their better photoemission and longer lifetime. Meanwhile, NEA InGaAs photocathodes have also become a promising candidate to obtain red-extended response, which is crucial for the design of near-infrared image intensifier. The response threshold of image intensifier using InGaAs material matches better with the night airglow than that of image intensifiers using traditional GaAs material, which can only extend to nearly 0.9 μm [11,12]. As a result, InGaAs-based image intensifier permits greatly-enhanced utilization of night airglow.

In order to effectively reduce the surface barrier for photoemission and obtain a true NEA state, the vacuum energy level of NEA photocathodes should be lower than the lowest unoccupied molecular orbital (LUMO) level. Many methods have been put forward for photocathode activation, among which Cs-only adsorption or Cs/O co-adsorption on *p*-type semiconductor surface is the most commonly used technique. Notably, Fisher et al. described in detail the NEA photoemission process of $In_xGa_{1-x}As$ alloys ($0 \leq x \leq 0.52$) and concluded that Cs-only adsorption on (001) surface of GaAs photocathode can only lead to zero electron affinity (ZEA) while a

* Corresponding author. and requested for materials:
E-mail address: yshen1016@foxmail.com (Y. Shen).

https://doi.org/10.1016/j.jallcom.2020.154869
0925-8388/

second-stage, Cs/O co-adsorption process may lower the electron affinity to negative values [13]. Machuca et al. investigated the surface energy bands and electron affinity of GaN photocathodes after activation and found that Cs-only process is enough for the attainment of the NEA state [14]. Further experimental and theoretical results confirmed that the activation process of AlGaN photocathodes is similar to that of GaN [15,16]. Chen et al. studied the Cs/O activation and photoemission properties of $Al_{0.63}Ga_{0.37}As$ photocathodes and evaluated the surface associated with the two activation stages [17]. Despite these prior efforts, the activation mechanism of InGaAs photocathodes remains unexplored. Given the importance of InGaAs photocathodes in near-infrared applications, investigation in the photoemission characteristics of Cs/O co-adsorbed InGaAs photocathodes is urgently needed.

Fisher et al. has pointed out that the lattice match between $In_xGa_{1-x}As$ and InP is related with the Indium component [13], and the lattice of $In_xGa_{1-x}As$ matches well with the InP substrate when x is 0.53. From a practical point of view, spectral response of the infrared-extension image intensifier which uses $In_{0.53}Ga_{0.47}As$ as the photo-emissive layer of the NEA photocathode matches the spectrum of night airglow perfectly. Meanwhile, potential applications in the field of narrow band-gap optoelectronic devices have also prompted active research on $In_{0.53}Ga_{0.47}As$/InP systems recent years [18–21]. Prior work indicates that As-terminated GaAs (001) β_2 (2 × 4) surfaces possess the lowest work function, lowest formation energy and highest sensitivity among all the possible candidates of α (2 × 4), β (2 × 4), β_2 (2 × 4), γ (2 × 4) reconstruction surfaces [22–26]. Considering the similarities between the structures of InGaAs (001) surface and GaAs (001) surface, $In_{0.53}Ga_{0.47}As$ (001) β_2 (2 × 4) surface has been chosen to simulate the InGaAs photocathode surface for further investigation.

In this paper, the effects of Cs/O co-adsorption on InGaAs photocathode surface are investigated in detail by using first-principles calculations combined with the experimental verifications. Adsorption energies, dipole moments, work functions, density of states, band structures and electron affinity with different adsorption models are calculated and analyzed. Photocathode activation experiments have also been performed, and the photocurrents during Cs-only and Cs/O activation processes are monitored by means of a multi-information on-line testing system [27]. Finally, schematic diagrams of energy bands and surface barrier heights are drawn to show the variation of electron affinity clearly. The motivation is to provide a comprehensive physical picture for further research on near-infrared NEA photocathodes and for expedited development of practical uses.

2. Calculated and experimental details

Our first-principles theory is based upon density-functional-theory (DFT) calculations, which are performed by means of the plane-wave-based Cambridge Sequential Total Energy Package (CASTEP) [28,29]. The Perdew-Burke-Ernzerhof (PBE) functional within the generalized gradient approximation (GGA) is used to describe the exchange-correlation interaction between electrons [30,31]. The calculation model features a set of plane-wave basis with a cutoff energy of 500 eV, which is sufficient for the calculation accuracy. The valence electronic configurations of the ultrasoft pseudopotentials for different atoms are as follows: In: $4d^{10}5s^25p^1$, Ga: $3d^{10}4s^24p^1$, As: $3d^{10}4s^24p^3$, Cs: $5s^25p^66s^1$, O: $2s^22p^4$ and H: $1s^1$. Geometry optimization is performed by using the Broyden-Fletcher-Goldfarb-Shanno (BFGS) algorithm and the SCF convergence criteria for structural optimization is set to be 2×10^{-6} eV/atom for energy change, 10^{-3} eV/nm for maximum force, 0.02 GPa for maximum stress, and 10^{-5} nm for change in displacement. Pseudo-hydrogen atoms are used to saturate the dangling bonds on the back surface [32]. The vacuum space along the z direction is set as 15 Å to eliminate the interaction of the neighboring slabs. The first Brillouin zone is sampled using 4 × 6 × 1 Monkhorst-Pack k-points mesh for optimizing the calculation structure [31]. The optimized substrate model with the best symmetry and the lowest formation energy used for further co-adsorption investigation (depicted in Fig. 1) is presented in the literature [33].

The reflection-mode InGaAs photocathode samples used in the experiments were fabricated on high-quality, (100)-oriented n-type InP substrates using the MOCVD technique. The 2-μm-thick InP buffer layer was designed to decrease the back-interface recombination velocity, and further improve the lattice quality. A Cs/O adlayer was covered on the surface of the InGaAs emission layer to activate the photocathodes. In order to eliminate contaminants on the photocathode surfaces, the samples underwent two cleaning steps before activation, which consist of chemical cleaning and thermal annealing. Firstly, the samples were etched by a mixed solution of HCl (38%) and de-ionized water with the ratio of 1:1 for 5 min. Following the chemical treatment, thermal annealing was performed at 525 °C for 20 min in an ultrahigh vacuum (UHV) chamber with a sub-10-8 Pa base pressure. These two cleaning steps ensure atomically clean surfaces on all samples. After that, Cs/O activation was carried out in the ultra-high-vacuum chamber upon the photocathode samples cooling down to the room temperature. The specific process of Cs and O sources introduced into the chamber could be referred to Ref. [13,34]. Once the fabrication is finished, the photocathodes were removed from the ultra-high-vacuum chamber and put to test. A negative bias voltage was added to the InGaAs photocathode samples, and the photocurrent was recorded under the illumination of a halogen tungsten lamp of 12 V/50 W.

3. Results and discussion

3.1. Surface adsorption energy

The structural stability of the Cs/O co-activation systems must be evaluated first by comparing the surface adsorption energy of each models. Surface adsorption energy is defined as [35]:

$$E_{ads} = E_{total} - E_{substrate} - n\mu_{Cs} - m\mu_O, \quad (1)$$

where E_{ads}, E_{total} and $E_{substrate}$ are the surface adsorption energy, the total energies of the co-adsorption models and the clean $In_{0.53}Ga_{0.47}As$ (001) β_2 (2 × 4) surface, respectively. μ_{Cs} and μ_O are the chemical potential of Cs and O atoms, respectively. n and m are the number of adsorbed Cs and O atoms, respectively. Considering thermodynamic equilibrium, the chemical potentials of Cs and O atoms are related by

$$2\mu_{Cs} + \mu_O = \mu_{Cs_2O}^{bulk}, \quad (2)$$

where $\mu_{Cs_2O}^{bulk}$ is the chemical potential of bulk Cs_2O. To ensure the stable surfaces, the following boundary conditions must be satisfied:

$$\mu_{Cs} \le \mu_{Cs}^{bulk},\ \mu_O \le \mu_{O_2}^{molecule}, \quad (3)$$

Due to the nature of Cs-rich surface, we treat μ_{Cs} as the same as that of Cs bulk. Accordingly, $\mu_O = \mu_{Cs_2O}^{bulk} - 2\mu_{Cs}^{bulk}$, the calculated surface adsorption energies are shown in Fig. 2(a). The negative E_{ads} indicates that the stability of the co-adsorption models is enhanced. Yu has pointed out that Cs—O atoms forming a 45° angle along the z axis of the $Al_{0.5}Ga_{0.5}As$ substrate are most suitable for further

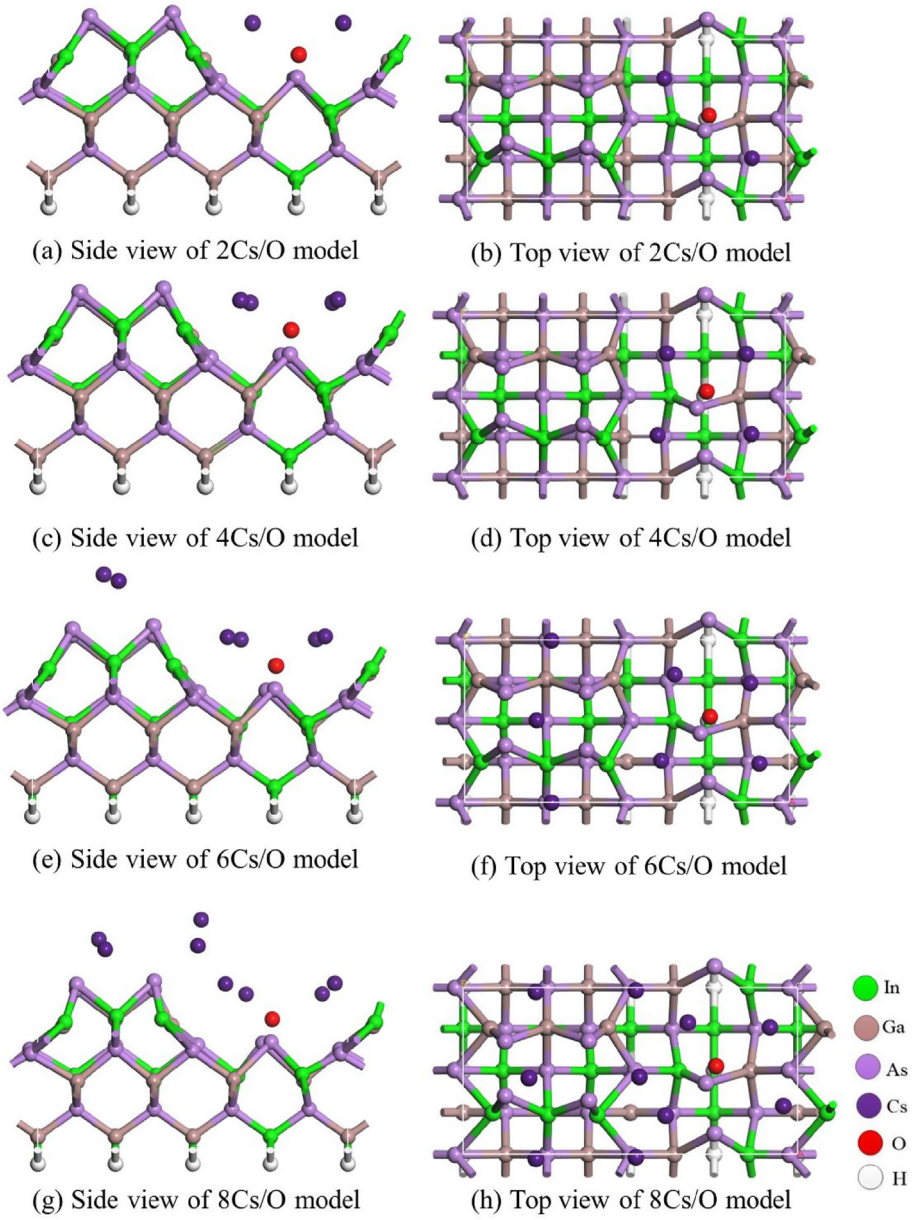

Fig. 1. Atomic structures of Cs/O co-adsorption on the As-terminated $In_{0.53}Ga_{0.47}As$ (001) β_2 (2×4) surface after geometry optimization. (a, c, e and g) represent the top view of 2Cs/O, 4Cs/O, 6Cs/O and 8Cs/O models while (b, d, f and h) show the side view of these models respectively.

adsorption process due to the lowest adsorption energy associated with such a structure [36]. We have built the same angle-dependent models to examine whether this conclusion applies to the InGaAs structure. The calculated adsorption energies of 0°, 45°, 90°, and 180° structures are −2.613 eV, −3.032 eV, −2.375 eV and 2.684 eV, respectively. Therefore, Cs−O-45° adsorption structure is adopted in this paper, as shown in Fig. 1. O atoms are fixed at the concave site while the Cs atoms mainly locate around O atoms and the positions of Cs atoms are higher than that of O atoms. As can be seen from Fig. 2(a), the co-adsorption models are all stable. O atoms become easier to be adsorbed as the number of Cs atoms increases. However, the stability slightly decreases when the Cs coverage exceeds 0.75 ML. Compared to first stage of Cs-only activation process [33], the overall structural stability of Cs/O co-adsorption is greatly enhanced.

3.2. Work function and surface dipole moments

Photoemission from an NEA photocathode surface can be described by a 'three-step' emission model [37] which consists of photoelectron excitation, electron transportation, and electron escaping into the vacuum. The excited photoelectrons need to overcome the energy barrier before escaping into the vacuum. In fact, the aim of activation process is to lower the energy barrier, and further contributes to acquire NEA state. Thus, work function is the key parameter to measure the quantum efficiency of photoemitters and can be defined as [38]:

$$\phi = E_{vac} - E_f, \tag{4}$$

where E_{vac} and E_f represent the energy of vacuum level and Fermi level, respectively. The calculated work functions of clean surface

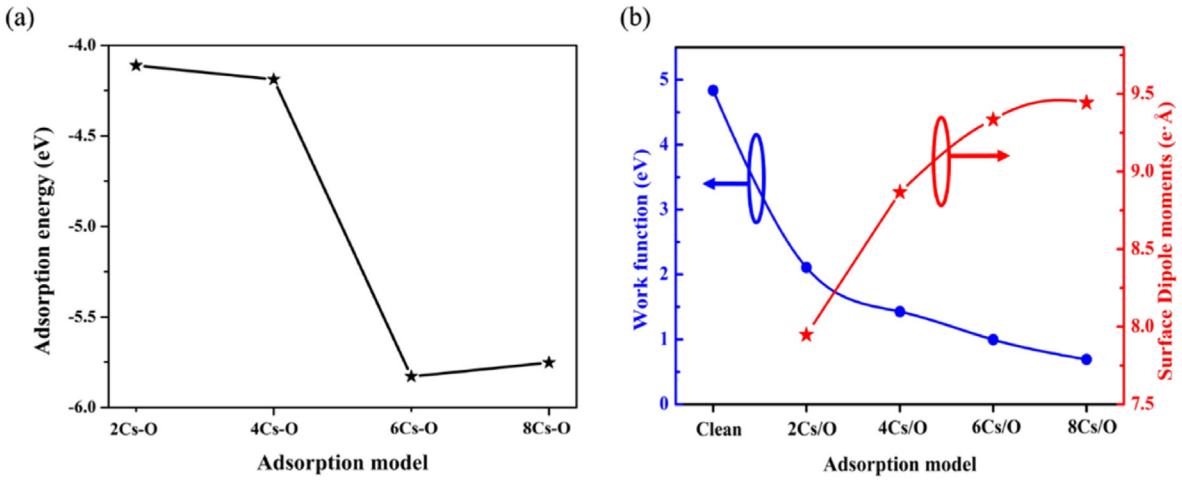

Fig. 2. Calculated adsorption energies, work functions and surface dipole moments of different Cs/O co-adsorption models.

and different co-activation models are shown in Fig. 2(b). Based on our previous research, Cs-only adsorption on InGaAs photocathode surface can significantly lower the work function [33]. However, the electron affinity remains positive under the Cs-only procedure, which is different from GaAs and GaN photocathodes [13,14]. After O adsorption, the work function is reduced by 2.279 eV, 3.408 eV, 3.840 eV and 4.144 eV, respectively. The work function of the 8Cs/O co-adsorption model is 0.692 eV, lower than the theoretical band gap of bulk $In_{0.53}Ga_{0.47}As$ (0.749 eV according to prior theoretical analysis [39]), indicating that the vacuum level is indeed below the LUMO, and the true NEA state can be achieved. The work function reaches the minimum value at the Cs coverage of 0.75 ML and then rises again during the Cs-only process. On the other hand, when O adatoms are present, the work function decreases monotonously as Cs coverage increases. Obviously, O adsorption plays an indispensable role in the activation of InGaAs photocathodes, and the incorporation of O atoms is conductive to the work function decreasing, and further improve the performance of photoemission.

Electrons redistribution between adatoms and the substrate surface leads to the change of work function and the formation of dipoles. Hogan et al. [40] have proposed a method to analyze the adatom-induced dipoles by taking the charge redistribution caused by adsorption into consideration. The charge difference $\Delta\rho(r)$ is defined as a function of spatial position:

$$\Delta\rho(r) = \rho_{adatom}(r) + \rho_{InGaAs}(r) - \rho_{adatom/InGaAs}(r), \tag{5}$$

where $\rho_{adatom}(r)$ is the electron density of isolated Cs or O atoms, $\rho_{InGaAs}(r)$ and $\rho_{adatom/InGaAs}(r)$ represent the total electron density of the InGaAs photocathode surfaces before and after Cs/O co-adsorption, respectively, and r is the spatial location in the different adsorption models. The average positive and negative dipole charge $Q^{\pm}$ and the average dipole length d_z normal to the surface can be calculated as:

$$\left.\begin{aligned} Q^{+} &= \sum_{z}\Delta\rho(r_z),\ (\Delta\rho(r_z) > 0) \\ Q^{-} &= \sum_{z}\Delta\rho(r_z),\ (\Delta\rho(r_z) < 0) \end{aligned}\right\}, \tag{6}$$

$$Q^{\pm} = Q^{+} + Q^{-}, \tag{7}$$

$$d_z = \frac{\sum_z \Delta\rho(r_z)z}{Q^{+}}\bigg|_{\Delta\rho(r_z)>0} - \frac{\sum_z \Delta\rho(r_z)z}{Q^{-}}\bigg|_{\Delta\rho(r_z)<0}, \tag{8}$$

where z represents the coordinate value of the z axis. Then the average dipole moments can be expressed as:

$$p_z = |Q^{\pm}| \times d_z \tag{9}$$

The calculated average dipole moments of different models are also depicted in Fig. 2(b). Obviously, the behaviors of dipole moment are in good agreement with the work function variation.

In order to explain the variations of work function and dipole moments, averaged E-Mulliken atom charge distributions of the co-adsorption models are calculated and listed in Table 1. In the Cs-only procedure, Cs loses electrons to surface atoms, leading to a dipole moment pointing from the surface to adatoms. With Cs coverage increases, the amount of charge transfer for each Cs atom decreases, resulting in an increase of surface electrons obtained from Cs adatoms. With O adsorption, the average positive charges, which include the Cs, In and Ga atoms, increased and the negative charges, i.e. As atoms, are increased as well. The electrons obtained by the O adatoms from the adatoms and the surface Ga and In atoms are transferred to surface As atoms. This charge redistribution between surface atoms and O adatom gives rise to the variation of sp3 hybrid orbitals.

Based on above analysis, the relationship between the adatoms and the substrate could be well clarified through the classical dipole model proposed by Su et al. [41]. The schematic diagram of dipole moments formed during the activation process of NEA InGaAs photocathode is depicted in Fig. 3. In the Cs-only stage, Cs atoms transfer a portion of electrons to the $In_{0.53}Ga_{0.47}As$ (001) reconstruction surface, forming the first dipole [Cs^{n+}-

Table 1
Calculated averaged E-Mulliken atom charge distribution, the positive value represents the electron donors while the negative value indicates the electron acceptors respectively.

	2Cs	2Cs/O	4Cs	4Cs/O	6Cs	6Cs/O	8Cs	8Cs/O
Cs	0.797	0.813	0.658	0.702	0.597	0.679	0.494	0.551
O	/	−1.168	/	−1.221	/	−1.202	/	−1.216
In	0.582	0.599	0.601	0.606	0.606	0.612	0.607	0.608
Ga	0.544	0.552	0.546	0.556	0.549	0.561	0.547	0.565
As	−0.518	−0.576	−0.579	−0.636	−0.649	−0.686	−0.663	−0.703

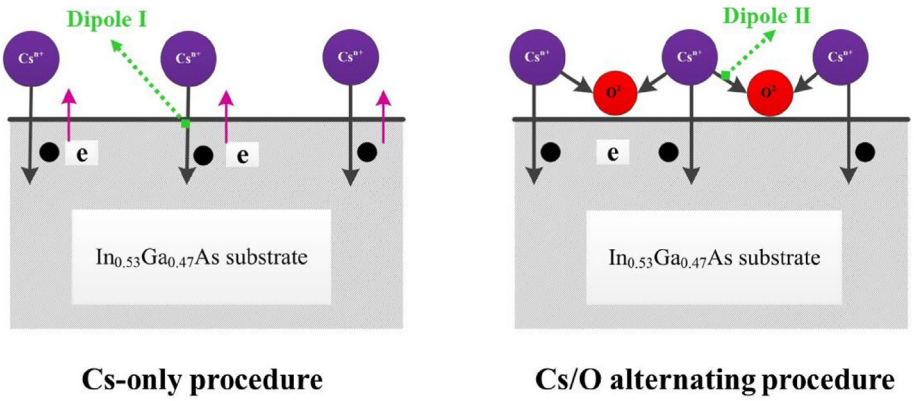

Fig. 3. Schematic diagram of dual-dipole models formed during the activation process of InGaAs photocathodes.

$In_{0.53}Ga_{0.47}As^{n-}$] forms (Dipole I), which is in favor of the work function lowering and the photoemission improving. However, depolarization of the first dipole occurs when the surface is over-cesiated and some electrons return to the adlayer, causing the work function to increase again beyond the optimum Cs coverage of 0.75 ML. In the Cs/O alternating stage, however, O atoms tend to acquire two electrons from Cs atoms to form O^{2-} ions, which can easily diffuse into the pores between the Cs adatoms due to their small sizes. As a result, a second dipole [Cs^{+}-O^{2-}-Cs^{+}] (Dipole II) is formed. It resists the depolarization of the first dipole caused by Cs—Cs interaction and further reduces the electron affinity.

3.3. Band structure and DOS before and after co-adsorption

The calculated band structures of clean substrate surface, Cs-only and Cs/O co-activation processes are presented in Fig. 4, in which the energy of vacuum level of clean substrate surface is taken as the reference. Due to the well-known DFT bandgap underestimation, the calculated band gap of clean $In_{0.53}Ga_{0.47}As$ (001) β_2 (2×4) surface (0.107 eV) is 30%—50% lower than the experimental value [42,43]. However, it does not influence the overall analysis of the electronic structures. After Cs-only adsorption, the LUMO level and highest occupied molecular orbital (HOMO) level all move towards the lower energy side, which is beneficial to band bending. The metallic property and the band banding region (BBR) become increasingly apparent as Cs coverage increases, contributing to the escape of the photoelectrons. The LUMO level reaches the minimum value and then moves upwards slightly. This phenomenon could further explain the variation trend of work function during Cs-only procedure. The HOMO and LUMO level can further move downward and the BBR is enlarged due to the addition of O atoms, leading to the further reduction of the work function. The true NEA state of InGaAs photocathode can be achieved after the Cs/O co-activation process. New energy bands also appear in the deep valence band ranging from −24 eV to −18 eV after Cs-only and Cs/O co-activation process, as depicted in Fig. 5. The band structures of clean substrate model and the Cs-only activation process in the deep valence band are provided as references.

In order to gain a comprehensive insight into the characteristic of energy bands, total density of states of clean substrate model and Cs/O co-activation models are calculated and shown in Fig. 6 (a). Meanwhile, partial density of states (PDOS) of Cs and O atoms in the adatom-substrate systems are shown in Fig. 6(b) and (c), respectively. The valence band of clean substrate surface consists of the

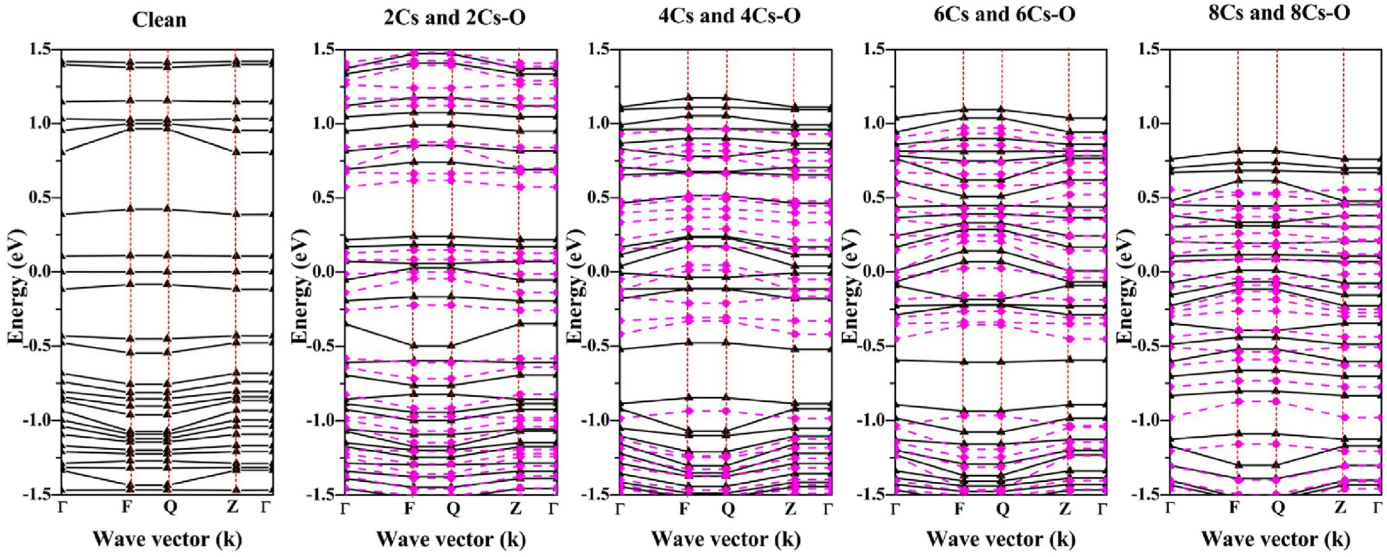

Fig. 4. Band structures of clean substrate surface, Cs-only and Cs/O co-activation models, the black solid line and magenta dotted line represent the Cs-only and Cs/O co-activation process, respectively. The vacuum level of clean substrate surface is used as the reference.

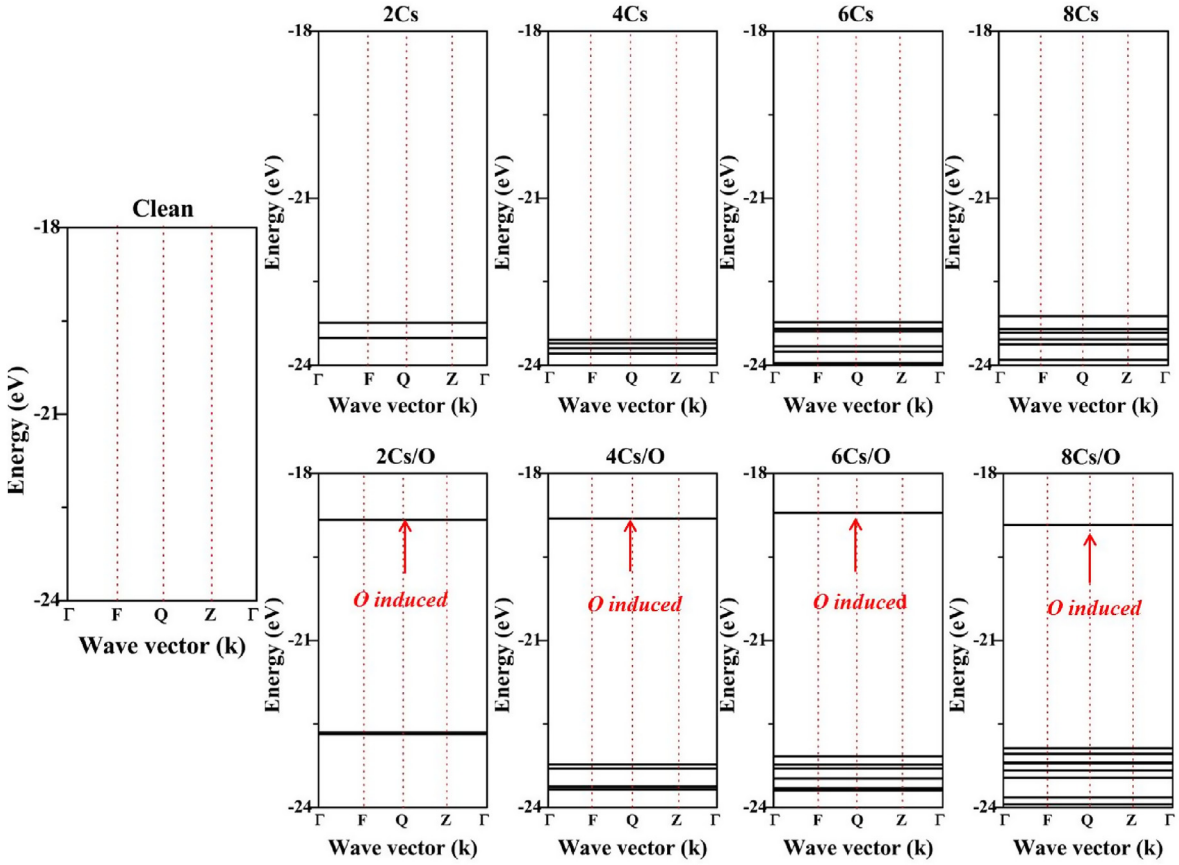

Fig. 5. New energy levels formed in the deep valence band during the Cs-only and Cs/O co-activation process. O-induced new energy bands in the deep valence band ranging from −19 eV to −18 eV are labelled using red arrows. (For interpretation of the references to colour in this figure legend, the reader is referred to the Web version of this article.)

lower valence band (−7 eV–0 eV) and the upper valence band (−16 eV to −9 eV), respectively. Due to the orbital hybridization, the TDOS near the Fermi level increases after Cs/O co-activation, contributing to the metallic property of the photocathode surface. In addition, new energy bands appear at −24 eV to −22 eV attribute to the Cs-5p state electrons and at −19 eV to −18 eV attribute to the joint effect of O-2s and O-2p state electrons. Cs adatoms mainly contribute to the upper valence band and the conduction band near the Fermi level while O adatoms have influence on the upper valence band.

3.4. Change of photocurrent during the activation process

The measured photocurrent of the R-mode $In_{0.53}Ga_{0.47}As$ photocathode is presented in Fig. 7. The entire curve comprises two stages: the first exposure to Cs and the subsequent Cs/O alternating process [44]. During the first stage, the photocurrent begins to rise after 9.6 min and then increases gradually with an increase in Cs coverage. The first peak value of 2.1 μA is achieved at around 12.9 min. Subsequently, the photocurrent begins to decline, indicating the occurrence of the "Cs-kill" phenomenon [45,46]. O source is turned on when the photocurrent is decreased to almost 85% of the peak value, and the photocurrent increases again. After that, the Cs/O alternative cycles are performed to further activate the photocathode samples.

The variation of surface barrier height of $In_{0.53}Ga_{0.47}As$ photocathode with Cs/O adlayer is shown in Fig. 8. During the first exposure to Cs, the vacuum level is gradually decreased as Cs coverage increases, and the distance between the vacuum and Fermi level is lowered accordingly. Surface barrier I is formed in this process. The reduced work function is indeed in favor of the escape of the photoelectrons, and thus the photocurrent can be increased. However, the work function goes up when the Cs source is in excess, leading to the decrease of the photocurrent. The lowest calculated work function of 2.842 eV is obtained at the optimum Cs coverage of 0.75 ML. Nevertheless, the band gap of bulk $In_{0.53}Ga_{0.47}As$ is 0.749 eV [39], which is much lower than the lowest work function, indicating the Cs-only process leads to the positive electron affinity (PEA) surface and there still exists a surface barrier height of 2.093 eV that needs to be overcome. The additional O source involved in the second stage of activation can dramatically lower the work function, contributing to the attainment of the true NEA state. The surface barrier II is formed during the Cs/O co-adsorption. The minimum work function is 0.692 eV after the Cs/O co-activation process, which is lower than the LUMO level by 0.057 eV. In this case, the excited photoelectrons can emit into the vacuum easier, and the quantum efficiency can be greatly improved. The band bending of narrow bandgap semiconductors is smaller, resulting in higher surface barrier. Therefore, the NEA state can hardly be obtained under Cs-only activation. The calculation results are in good agreement with the experimental results.

4. Design rules in practice

Combined first-principles calculation with experimental verification, a reasonably thorough and useful account of surface activation of NEA $In_xGa_{1-x}As$ photocathodes have been put forward. Across all the NEA III-V photocathodes studied previously, the activation

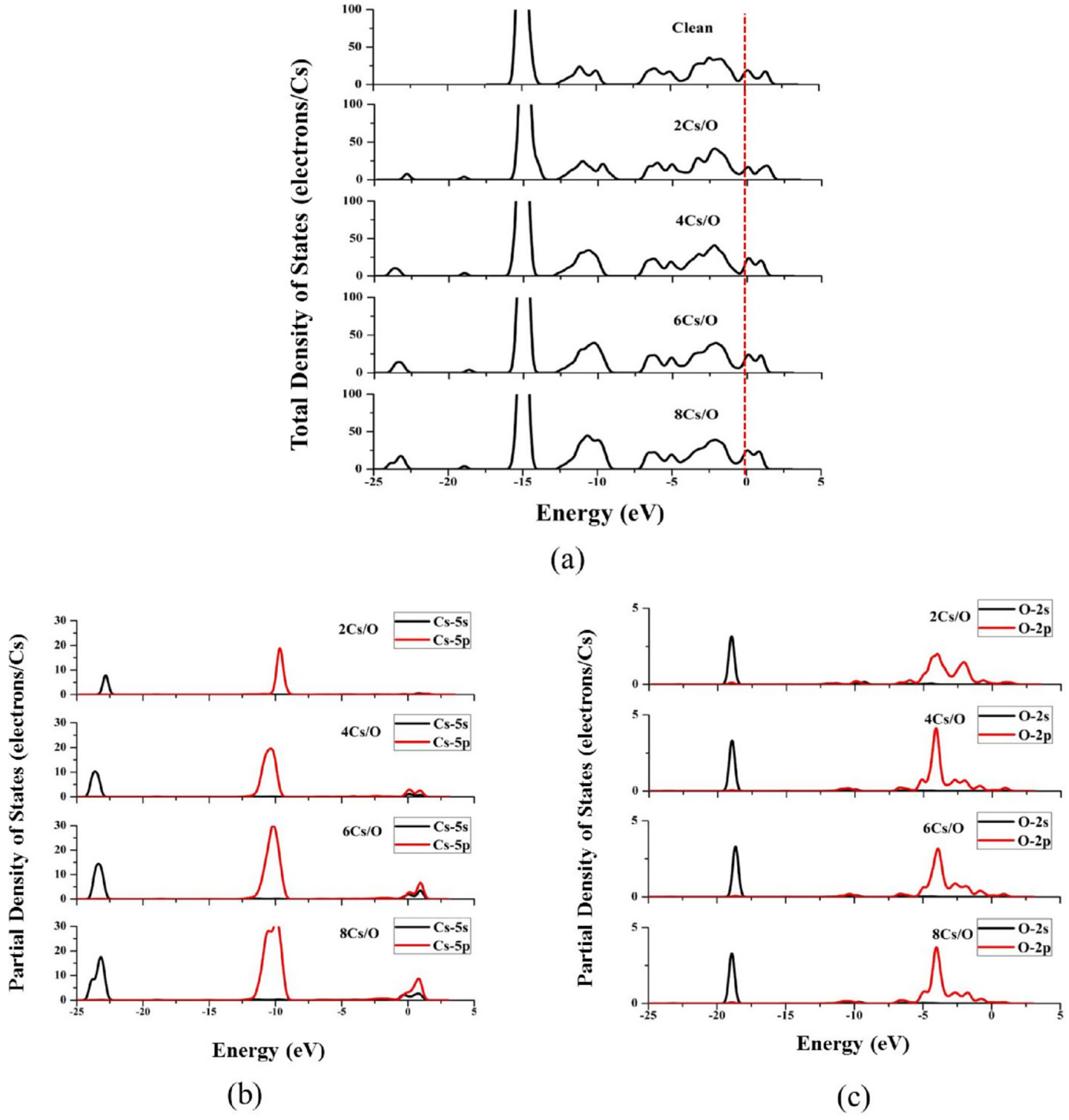

Fig. 6. TDOS of clean substrate surface and Cs/O co-adsorption models (a) and PDOS of Cs adatoms (b) and O adatoms (c).

process is the most significant determinant of the performance of NEA. Hence, when discussing the NEA characteristic of different III-V photocathodes, the first step is to determine the electron affinity after Cs-only activation by means of theoretical simulation. If the calculated vacuum level is still higher than the conduction band bottom, further Cs—O co-activation process is particularly important in order to obtain the NEA state. The next step is to implement the activation experiment using the empirical values obtained by first-principles, especially the relative amount of Cs and O sources released into the reactive chamber. Finally, the photocurrent and quantum efficiency curves of the photocathodes after activation are measured simultaneously. At this stage, the variation of the photocurrent can be well explained by the calculated work function.

5. Conclusions

In summary, first-principles calculations of Cs/O co-activation on (001) surface of near-infrared $In_{0.53}Ga_{0.47}As$ photocathode are

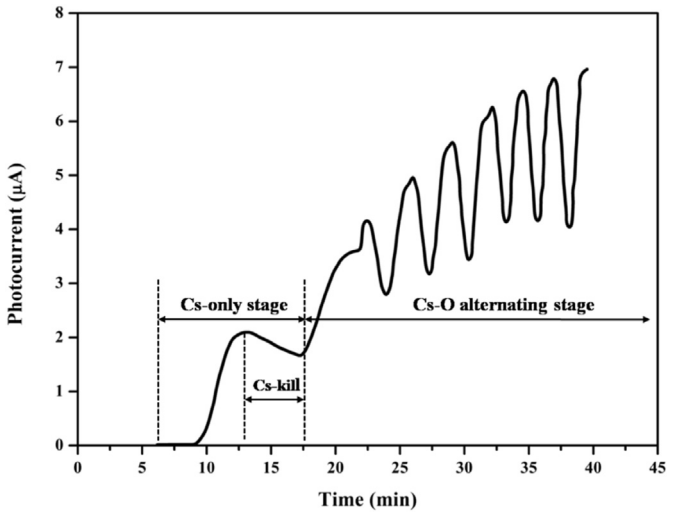

Fig. 7. Photocurrent variation of $In_{0.53}Ga_{0.47}As$ photocathode during Cs-only and Cs/O co-activation process.

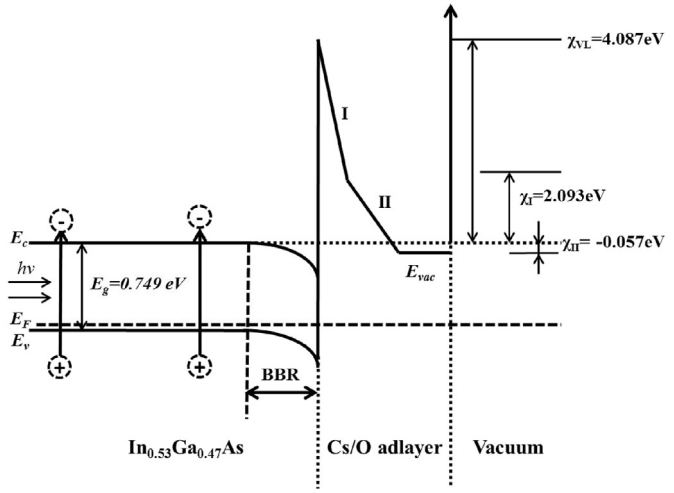

Fig. 8. Schematic energy band diagram showing the surface barrier height for the NEA $In_{0.53}Ga_{0.47}As$ photocathode. E_c and E_v represent the conduction and valence band respectively, E_F is the Fermi energy level, E_g is the band gap, E_{vac} is the vacuum level, and χ represent the electron affinity.

performed based on DFT, and Cs/O activation experiments are carried out on a R-mode InGaAs photocathode. Calculations results show that the structural stability is considerably enhanced after Cs/O adsorption, and the trend of stability variation differs from that of previously-studied Cs-only procedures. O adsorption plays an indispensable role in the achievement of true NEA InGaAs photocathode. The work function decreases simultaneously as Cs coverage increases after O adatoms are introduced. The formed second dipole [Cs^{+}-O^{2-}-Cs^{+}] resists the depolarization of the first dipole [Cs^{n+}-$In_{0.53}Ga_{0.47}As^{n-}$] and further reduces the electron affinity. The HOMO and LUMO levels further move toward the low energy region and the BBR enlarges as a result of oxygen incorporation. Meanwhile, new energy bands in the deep energy level appear due to the joint effect between adatoms. The photocurrent curve is monitored and recorded during the activation procedure. The variation trend of the photocurrent is in close correlation with the calculated work function, indicating the calculation results are well consistent with the experiments. This work reveals the Cs/O activation mechanism of InGaAs photocathodes from the perspectives of both theory and experiment. It may offer valuable guidance to the design and fabrication of $In_xGa_{1-x}As$ photocathode with high quantum efficiencies.

Declaration of competing interest

The authors declare that they have no known competing financial interests or personal relationships that could have appeared to influence the work reported in this paper.

CRediT authorship contribution statement

Liang Chen: Methodology, Writing - original draft. **Yang Shen:** Conceptualization, Writing - review & editing, Supervision. **Xiaodong Yang:** Software, Methodology. **Muchun Jin:** Validation, Investigation. **Songmin Liu:** Formal analysis. **Lingze Duan:** Investigation, Visualization. **Shiqing Xu:** Resources, Project administration.

Acknowledgments

This work is supported by the National Natural Science Foundation of China (Grant NO. 61775203), the National Key Research and Development Program of China (Grant No. 2017YFF0210800) and Natural Science Foundation of Zhejiang Province (Grant No. LZ20F050001). The author also thanks Prof. S.L. Gu and J.G. Wan of Nanjing University for the help of DFT calculations.

References

[1] J.M. Roth, T.E. Murphy, C. Xu, Ultrasensitive and high-dynamic-range two-photon absorption in a GaAs photomultiplier tube, Opt. Lett. 27 (2002) 2076–2078.
[2] J. Wehmeijer, B. van Geest, High-speed imaging: image intensification, Nat. Photon. 4 (2010) 152–153.
[3] S. Uchiyama, Y. Takagi, M. Niigaki, H. Kan, H. Kondoh, GaN-based photocathodes with extremely high quantum efficiency, Appl. Phys. Lett. 86 (2005) 103511.
[4] T. Nishitani, M. Tabuchi, Y. Takeda, Y. Suzuki, K. Motoki, T. Meguro, High-Brightness spin-polarized electron source using semiconductor photocathodes, Jpn. J. Appl. Phys. 48 (2009), 06FF02.
[5] E.J. Tarsa, P. Kozodoy, J. Ibbetson, B.P. Keller, G. Parish, Solar-blind AlGaN-based inverted heterostructure photodiodes, Appl. Phys. Lett. 77 (2000) 316–318.
[6] M.A. Dehn, K. Aulenbacher, V. Bechthold, F. Fichtner, Reducing the contribution of the photoemission process to the unwanted beam in photoelectron sources at accelerators, Appl. Phys. Lett. 111 (2017) 132105.
[7] L.B. Jones, H.E. Scheibler, D.V. Gorshkov, A.S. Terekhov, B.L. Militsyn, T.C.Q. Noakes, Evolution of the transverse and longitudinal energy distributions of electrons emitted from a GaAsP photocathode as a function of its degradation state, J. Appl. Phys. 121 (2017) 225703.
[8] J.J. Zou, X.W. Ge, Y.J. Zhang, W.J. Deng, Z.F. Zhu, W.L. Wang, X.C. Peng, Z.P. Chen, B.K. Chang, Negative electron affinity GaAs wire-array photocathodes, Optic Express 24 (2016) 4632–4639.
[9] C. Feng, Y.J. Zhang, Y.S. Qian, B.K. Chang, F. Shi, G.C. Jiao, J.J. Zou, Photoemission from advanced heterostructured $Al_xGa_{1-x}As$/GaAs photocathodes under multilevel built-in electric field, Optic Express 23 (2015) 19478–19488.
[10] X.G. Jin, B. Ozdol, M. Yamamoto, A. Mano, N. Yamamoto, Y. Takeda, Effect of crystal quality on performance of spin-polarized photocathode, Appl. Phys. Lett. 105 (2014) 203509.
[11] M.M. Dougal, A. Hood, J. Geske, J. Wang, F. Patel, D. Follman, J. Manzo, J. Getty, InGaAs focal plan arrays for low light level SWIR imaging, Proc. SPIE 8012 (2011) 801221.
[12] H. Inada, H. Mori, Y. Nagai, MOVPE grown InGaAs/GaAsSb Type II quantum well photodiode for SWIR focal plane array, Proc. SPIE 8012 (2011) 801220.
[13] D.G. Fisher, R.E. Enstrom, J.S. Escher, B.F. Williams, Photoelectron surface escape probability of (Ga, In)As : Cs–O in the 0.9 to 1.6 μm range, J. Appl. Phys. 43 (1972) 3815–3823.
[14] F. Machuca, Y. Sun, Z. Liu, K. Ioakeimidi, P. Pianetta, R.F.W. Pease, Prospect for high brightness III-nitride electron emitter, J. Vac. Sci. Technol. B 18 (2000) 3042–3046.
[15] Y.J. Zhang, J.J. Zou, X.H. Wang, B.K. Chang, Y.S. Qian, J.J. Zhang, P. Gao, Comparison of the photoemission behaviour between negative electron affinity GaAs and GaN photocathodes, Chin. Phys. B 20 (2011), 048501.

[16] M.Z. Yang, B.K. Chang, M.S. Wang, Cesium, oxygen coadsorption on AlGaN(0001) surface: experimental research and ab initio calculations, J. Mater. Sci. Mater. Electron. 26 (2015) 2181–2188.
[17] X.L. Chen, J. Zhao, B.K. Chang, X.H. Yu, G.H. Hao, Y. Xu, H.C. Cheng, Photoemission characteristics of (Cs, O) activation exponential-doping $Ga_{0.37}Al_{0.63}As$ photocathodes, J. Appl. Phys. 113 (2013) 213105.
[18] N. L Rowell, G. Yu, D.J. Lockwood, P.J. Poole, Phonons in $In_{0.53}Ga_{0.47}As$/InP(100) superlattices by infrared reflectance, Phys. Rev. B 68 (2003) 165320.
[19] C. Mukherjee, T. Das, C. Mahata, C.K. Maiti, C.K. Chia, S.Y. Chiam, D.Z. Chi, G.K. Dalapati, Interface properties of atomic layer deposited TiO_2/Al_2O_3 films on $In_{0.53}Ga_{0.47}As$/InP substrates, ACS Appl. Mater. Interfaces 6 (2014) 3263–3274.
[20] W.R. Clark, K. Vaccaro, W.D. Waters, C.L. Gribbon, B.D. Krejca, Determination of quantum efficiency in $In_{0.53}Ga_{0.47}As$-InP-based APDs, J. Lightwave Technol. 32 (2014) 4780–4784.
[21] N.K. Saini, S. Sahay, R.S. Saxena, M.J. Kumar, $In_{0.53}Ga_{0.47}As$/InP trench-gate power MOSFET based on impact ionization for improved performance: design and analysis, IEEE Trans. Electron. Dev. 64 (2017) 4561–4567.
[22] D.K. Biegelsen, R.D. Bringans, J.E. Northrup, L.E. Swartz, Surface reconstructions of GaAs(100) observed by scanning tunneling microscopy, Phys. Rev. B 41 (1990) 5701–5706.
[23] T. Hashizume, Q.K. Xue, J. Zhou, A. Ichimiya, T. Sakurai, Structures of as-rich GaAs(001)-(2 × 4) reconstructions, Phys. Rev. Lett. 73 (1994) 2208–2211.
[24] T. Hashizume, Q.K. Xue, A. Ichimiya, T. Sakurai, Determination of the surface structures of the GaAs(001)-(2×4) As-rich phase, Phys. Rev. B 51 (1995) 4200–4212.
[25] L.D. Broekman, R.C.G. Leckey, J.D. Riley, A. Stampfl, B.F. Usher, B.A. Sexton, Scanning-tunneling-microscope study of the α and β phases of the GaAs (001)-(2×4) reconstruction, Phys. Rev. B 51 (1995) 17795–17799.
[26] W.G. Schmidt, F. Bechstedt, Geometry and electronic structure of GaAs(001)(2×4) reconstructions, Phys. Rev. B 54 (1996) 16742–16748.
[27] J.J. Zou, L. Feng, G.Y. Lin, Y.T. Rao, Z. Yang, Y.S. Qian, B.K. Chang, On-line measurement system of GaAs photocathodes and its applications, Proc. SPIE 6782 (2007) 67823D.
[28] H.P. Komsa, E. Arola, J. Pakarinen, S.P. Chang, T.T. Rantala, Beryllium doping of GaAs and GaAsN studied from first principles, Phys. Rev. B 79 (2009) 115208.
[29] L.X. Zhang, W.E. McMahon, S.H. Wei, Passivation of deep electronic states of partial dislocations in GaAs: a theoretical study, Appl. Phys. Lett. 96 (2010) 121912.
[30] J.P. Perdew, A. Zunger, Self-interaction correction to density-functional approximations for many-electron systems, Phys. Rev. B 23 (1981) 5048.
[31] J.P. Perdew, K. Burke, M. Ernzerhof, Generalized gradient approximation made simple, Phys. Rev. Lett. 77 (1996) 3865–3868.
[32] S. Krukowski, P. Kempisty, P. Strak, Electrostatic condition for the termination of the opposite face of the slab in density functional theory simulations of semiconductor surfaces, J. Appl. Phys. 105 (2009) 113701.
[33] Y. Shen, X.D. Yang, Y. Bian, L. Chen, K. Tang, J.G. Wan, R. Zhang, Y.D. Zheng, S.L. Gu, Early stage of Cs activation mechanism for $In_{0.53}Ga_{0.47}As$ (001) β_2 (2×4) surfaces: insights from first-principles calculations, Appl. Surf. Sci. 457 (2018) 150–155.
[34] Y. Sun, Z. Liu, P. Pianetta, D. Lee, Formation of cesium peroxide and cesium superoxide on InP photocathode activated by cesium and oxygen, J. Appl. Phys. 102 (2007), 074908.
[35] J.R. Kitchin, Correlations in coverage-dependent atomic adsorption energies on Pd(111), Phys. Rev. B 79 (2009) 205412.
[36] X.H. Yu, A density functional theory research on Cs–O activation process of GaAlAs photocathodes, J. Mater. Sci. 51 (2016) 8259–8269.
[37] W.E. Spicer, A. Herrera-Gomez, Modern theory and applications of photocathodes, Proc. SPIE 2022 (1993) 18.
[38] A.L. Rosa, J. Neugebauer, First-principles calculations of the structural and electronic properties of clean GaN(0001) surfaces, Phys. Rev. B 73 (2006) 205346.
[39] K. Shim, Principal band gaps and bond lengths of the alloy $(Al_xGa_{1-x})_{1-z}In_zP_yAs_{1-y}$ lattice matched to GaAs, Thin Solid Films 516 (2008) 3143–3146.
[40] C. Hogan, D. Paget, Y. Garreau, M. Sauvage, G. Onida, L. Reining, P. Chiaradia, V. Corradini, Early stages of cesium adsorption on the As-rich(2×8) reconstruction of GaAs(001): adsorption sites and Cs-induced chemical bonds, Phys. Rev. B 68 (2003) 205313.
[41] C.Y. Su, W.E. Spicer, I. Lindau, Photoelectron spectroscopic determination of the structure of (Cs,O) activated GaAs (110) surfaces, J. Appl. Phys. 54 (2007) 1413–1422.
[42] W.E. Pickett, Pseudopotential methods in condensed matter applications, Comput. Phys. Rep. 9 (1989) 115–198.
[43] P. Rinke, M. Scheffler, A. Qteish, M. Winkelnkemper, D. Bimberg, J. Neugebauer, Band gap and band parameters of InN and GaN from quasi-particle energy calculations based on exact-exchange density-functional theory, Appl. Phys. Lett. 89 (2006) 161919.
[44] V.V. Bakin, K.V. Toropetsky, H.E. Scheibler, A.S. Terekhov, L.B. Jones, B.L. Militsyn, T.C.Q. Noakes, p-GaAs(Cs,O)-photocathodes: demarcation of domains of validity for practical models of the activation layer, Appl. Phys. Lett. 106 (2015) 183501.
[45] G.V. Benemanskaya, V.S. Vikhnin, N.M. Shmidt, G.E. Frank-Kamenetskaya, I.V. Afanasiev, Electron accumulation layer at the Cs-covered GaN(0001) n-type surface, Appl. Phys. Lett. 85 (2004) 1365–1367.
[46] X.H. Wang, B.K. Chang, Y.J. Du, J.L. Qiao, Quantum efficiency of GaN photocathode under different illumination, Appl. Phys. Lett. 99 (2011), 042102.